Integration and optimization of the after-treatments systems to reduce the acoustic footprint of the ships

Giada Kyaw Oo D'Amore [a,*], Mitja Morgut [a], Marco Biot [a], Francesco Mauro [b], Jan Kašpar [c]

[a] University of Trieste, Engineering and Architecture Department, Via Alfonso Valerio 6, 34127 Trieste, Italy
[b] Sharjah Maritime Academy, 180018, Khorfakkan, Sharjah, United Arab Emirates
[c] University of Trieste, Department of Chemical and Pharmaceutical Science, Via L. Giorgieri 1, 34127 Trieste, Italy

ARTICLE INFO

Keywords:
After-treatments systems
CFD
FEM
Genset mock-up
Noise emissions
Chemical emissions
Systems integration

ABSTRACT

Exhaust Gas Cleaning Systems (EGCS) such as scrubbers are mandatory and extensively used to abate SOx in exhaust gases when high sulphur content fuel oil is employed in the marine engine in order to comply with international ship emission regulations, both in new and existing ships. Currently, about 13% of bulker, container, and tanker ships have a scrubber installed, despite the fact that their installation on board is challenging due to their large dimensions to be fitted into the funnel and the complexity of the system, since the exhaust line must control both the chemical and acoustic emissions. In the presented work a combined FEM, CFD simulations and GA optimization methodology aimed at the integration of the abatement system, while optimizing the acoustic properties, is developed. The methodology is first assessed on an industrially-relevant scenario that involves the use of a Genset mock-up equipped with a reference Diesel Oxidation Catalyst (DOC) and a scrubber for the abatement of both NOx and SOx, showing that acoustic performances of the DOC are reliably modelled by the FEM-CFD methodology, which has a significantly reduced computational cost as compared to conventional CFD modelling of acoustic properties. The GA optimization is carried out to improve the DOC acoustic properties showing that it is possible to confer the silencing effect to the after-treatment systems, thus eliminating the traditional silencers from the exhaust line. This leads to a compact exhaust line that integrates the EGCS while maintaining efficient both the chemical pollution abatement capability, and silencing effects to guarantee full compliance (*i.e.*, acoustic and chemical) with the international regulations.

1. Introduction

Maritime transport is of great importance for the global economy, as it accounts for around 80% of worldwide trade, together with its related activities (*e.g.,* shipbuilding, repairs, and port activities) [1]. Whereas shipping accounts for about 2.5% of global CO_2 emissions, due to the extensive use of heavy fuel oils, it heavily impacts polluting emissions: in 2018 the maritime transport accounted for 24% of each Sulphur (SOx) and Nitrogen Oxides (NOx) emissions in the EU economic area [2]. Therefore, there has been an increasing concern about the global impact of maritime emissions. Consistently, IMO (International Maritime Organization) has restricted both the worldwide SOx and NOx emission limits imposed by MARPOL 73/78 Annex VI Regulation [3] and those, more restrictive, in the emission control areas (ECAs), *i.e.,* NECAs (Nitrogen Emission Control Areas) or SECAs (Sulfur Emission Control Areas) [3].

NOx are generated at high temperatures in the combustion chamber of engines and systems such as EGR (Exhaust Gas Recirculation) and SCR (Selective Catalytic Reduction) are used on board for their abatement [4,5]. However, those solutions present some drawbacks: EGR increases PM (Particulate Matter) emissions and fuel consumption by about 4% [6], while SCR involves the use and storage of urea and the installation of an injection system along the exhaust line [7,8].

Since the amount of the SOx emissions linearly depends on the Sulphur content of the fuel, IMO pushed down the S %wt content of High Sulphur Fuel Oil, (HSFO; S <3.5 %wt), making use of fuels with low Sulphur content mandatory, *i.e.*, VLSFO - Very Low Sulphur Fuel Oil (S <0.5 wt%) and ULSFO - Ultra Low Sulphur Fuel Oil (S <0.1 wt%). The use of low Sulphur content combustibles significantly impacts the total ship operating costs, since 60% of them are associated with the fuel. For instance, on May 15th 2023, Rotterdam bunker prices for respectively HSFO, VLSFO, ULSFO, were 423 $/mt, 519 $/mt, and 787 $/mt [9],

highlighting the impact of the fuel cost on shipping. Accordingly, an alternative solution to ensure compliance with SOx regulations is the installation of scrubbers as Exhaust Gas Cleaning Systems (EGCS). Scrubbers represent a viable solution [10] and show a lower climate impact than low Sulphur fuels [11]. This aspect is confirmed also by EGCS manufacturers, which assert that the costs saved by using HSFO instead of LSFO or even ULSFO, can pay back the costs of installing and operating EGCS in about one year [6].

Ships emissions are not limited to chemical pollution; remarkable is also the importance of controlling and minimizing the exhaust gas noise. Several regulations and class notations [12–14] limit the perceived noise level at the decks of the ship and at prescribed distances from the vessels, during both the navigation and the mooring in ports. Diesel engines are the main sources of noise radiated by ships in the air: the noise generated in the combustion chamber propagates through the exhaust gas to the surroundings. To reduce the emitted noise, silencers are usually installed along the exhaust line [15,16]There are three basic requirements for a modern exhaust system: compact outer geometry, sufficient attenuation, and low-pressure drop. Sound in silencer can be attenuated by the use of sound-absorbing materials in which sound energy is converted into heat mainly by viscous processes, or the attenuation can be performed through the reflection of sound, which is caused by changes of the cross-section area or the use of different kinds of acoustic resonators. There are also cases where resistive and reactive properties are combined in the same silencer element.

The installation of SCR/EGR, scrubber and silencer onboard could represent a reliable technical solution to satisfy the limits imposed on both the chemical, *i.e.* NOx and SOx, and acoustic emissions, especially for the fleet of ships already in navigation, allowing the compliance with the international regulation without the need of an entire refitting of the propulsion system. However, those solutions are hardly applicable because of space limitations [17]; after-treatment systems have big dimensions and have to be installed in the funnel, where the space is limited. Accordingly, the integration of the necessary components of theeded after-treatment systems along the exhaust line becomes mandatory a key point in order to save space [4]. Prototypes of integrated SCR-silencer systems have been constructed [18], but,only a few literature studies of the acoustic performances of SCRs are reported [4,19]. Also for marine scrubber systems just a few literature studies s consider their acoustic properties [20] and no industrial prototypes are reported. On the contrary, the acoustic performances of silencers areare extensively studied, especially in the automotive industry [21–25], considering the influence of the shape of the silencer on noise reduction and generated back pressure. The acoustic properties of the silencers are usually studied and optimised using both FEM [26–28] and CFD [29–32] approaches; the first one considers the geometry as an influencing parameter, while the second one considers also the influence of the flow inside the silencer and calculates the pressure drop generated by the silencer as well. However, the CFD approach requires high computational costs due to the complexity of the modelling. Recently, a novel approach was proposed that combines FEM and CFD, which allows for reducing the computational burden of full CFD modelling were [24,33]. However, it is important to point out that these studies use simplified models that, for example, do not consider viscous dissipations in the acoustic simulations. Efficient and cost-effective numerical models produce benefits in terms of both time and costs for the optimization of the flow field along the exhaust line thus reducing the number of prototypes to be constructed and tested.

As above highlighted, the development of compact abatement systems capable of simultaneously reducing NOx, SOx and noise is of strong interest, due to the difficulty of combining SCR/EGR, scrubber and silencer technologies on a ship [17]. This work is carried out within the project ABE [34], which addresses the problem of simultaneous NOx and SOx abatement by using a combination of a Diesel Oxidation Catalyst (DOC) followed by a scrubber, besides the integration of the silencing effect into this technology. The DOC promotes the oxidation of Nitrogen Monoxide (NO), which is the main NOx species originated in the engine, enhancing NOx solubility [17,35]. The use of a DOC for NOx abatement requires less space in comparison to a traditional SCR and does not involve the use and storage of urea on board. Moreover, the presence of the DOC does not influence fuel consumption, in contrast to the EGR, and allows the abatement of carbon monoxide (CO), hydrocarbons (HC) and PM [35]. In order to test/verify the proposed technological solution, a pilot demonstrator has been constructed and tested at the University of Trieste. Here, the focus is on the modelling of its acoustic properties.

More precisely, the main objectives of this part of the project can be summarized in the following points:

- perform reliable measurements of acoustic properties of after-treatments systems on the Genset mock-up, considering the difficulties and the limits of the measurement procedure due to the test conditions (*e.g.*, high temperatures, turbulence flow, presence of particulate matter).
- develop a robust and computationally efficient numerical methodology to study acoustic properties of exhaust line components.
- optimize the acoustic properties of exhaust line components, while maintaining the constraints imposed by geometrical parameters, flow characteristics and the chemical reactions needed to satisfy NOx and SOx regulations.

Specifically, here the reference DOC is experimentally tested and numerically simulated to evaluate its acoustic performance in terms of Transmission Loss (*TL*). The experimental results are compared with the *TL* curves calculated using the proposed methodology, resulting in a good agreement. Then, the assessed numerical methodology is used to optimize the acoustic properties of the DOC, developing surrogate models of DOC performances using a Response Surface Methodology (RSM). Finally, an integrated system consisting of the optimized DOC followed by a scrubber prototype is evaluated to assess the possibility of eliminating the traditional silencer from the exhaust line.

2. Acoustic properties of the exhaust gas cleaning systems

2.1. The transmission loss as key performance index and measurement methodology

Several parameters describe the acoustic performance of a component. These include noise reduction (*NR*), insertion loss (*IL*), and *TL*. The *NR* is the sound pressure level difference across the silencer. Though the *NR* can be easily measured, it is not particularly helpful for silencer design. The *IL* is the sound pressure level difference at a point, usually outside the system, without and with the silencer present. Even though the *IL* is very useful to the industry, its modelling is difficult since it depends not only on the silencer geometry itself but also on the source and radiation impedances. The *TL* is the difference in the sound power level between the incident wave entering and the transmitted wave exiting the silencer when the silencer termination is anechoic, and can be expressed as follows [22]:

$$TL = 10\log_{10}\frac{W_i}{W_t} \tag{1}$$

where W_i and W_t are the incidents and the transmitted waves sound power, respectively. The benefit of *TL* is that it is a parameter characterizing only the silencer, without the need of evaluating or modelling the source or termination properties. Because of the simplifications, the *TL* is the most common parameter for silencer performance [22]. For this reason, the *TL* is used as Key Performance Index (KPI) instead of *IL* or *NR* in this study. Two methods are employed for its evaluation: the decomposition technique and the two-load technique for the numerical evaluation and the experimental measurements, respectively.

The decomposition method [36,37] measures acoustic properties in-

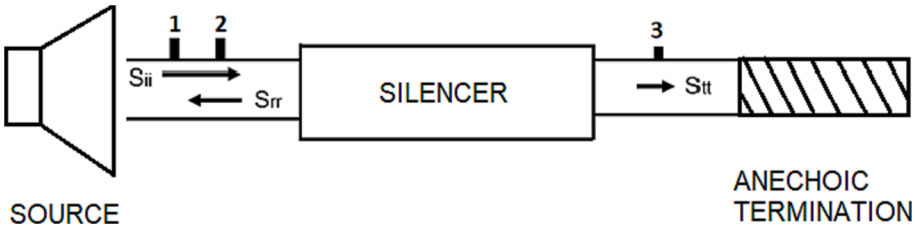

Fig. 1. Measurement set-up according to the decomposition theory.

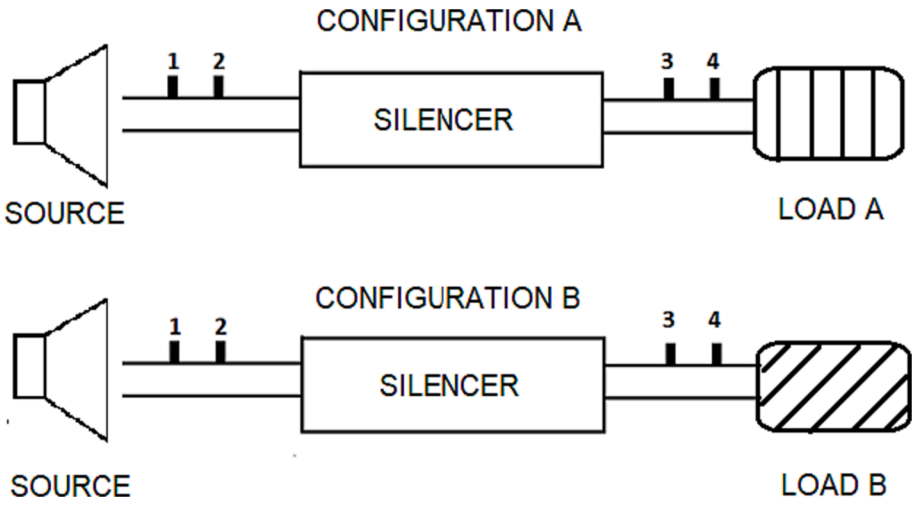

Fig. 2. Measurement set-up according to the two-loads method.

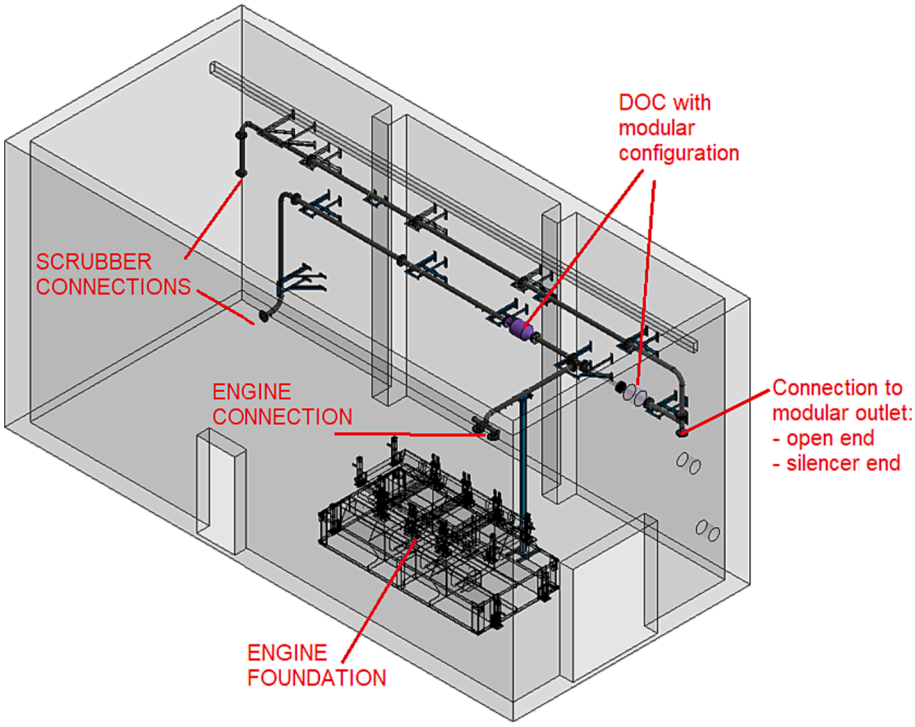

Fig. 3. Scheme of the experimental mock-up.

ducts using a measurement set-up as depicted in Fig. 1. S_{ii}, S_{rr}, and S_{tt} represent the auto-spectra of the incident, reflected and transmitted sound waves. Considering a plane wave propagation and using two microphones at locations 1 and 2, the sound pressure can be decomposed into its incident and reflected waves. The microphone at location 3 directly measures the transmitted sound pressure as the anechoic termination avoids reflection. The decomposition theory provides an expression for the auto-spectrum S_{ii} of the incident wave, so the

Table 1
4 S Genset characteristics.

Engine Model	N. of Cylinders	Bore × Stroke [mm]	RPM
IVECO 8361SRi26	6 in-line	115 × 130	1500

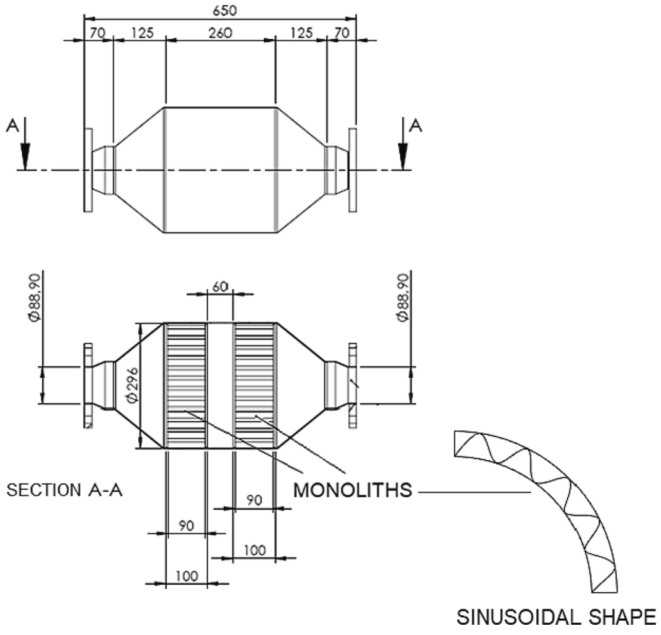

Fig. 4. Geometry of the reference DOC.

Table 2
Genset Iveco analytical *EFRs* and *CFRs*.

	1st order	2nd order	3rd order	4th order
EFR [Hz]	75	150	225	300
CFR [Hz]	12.5	25.0	37.5	50.0

sound power of incident and transmitted waves can be derived, and the *TL* can be expressed as follows [22]:

$$TL = 20log_{10}\frac{p_i}{p_t} + 10log_{10}\frac{S_i}{S_t} \tag{2}$$

where p_i and p_t are the RMS (Root Mean Square) pressure amplitude of the incident and transmitted sound waves, and S_i and S_t are the cross-section area of the silencer inlet and outlet pipe, respectively. The major drawback of the decomposition method is that a fully anechoic termination is difficult to reproduce in experiments, affecting the reliability of the *TL* measurement.

A silencer can also be modelled using the so-called four-pole parameters method [38]. The four parameters (*A*, *B*, *C* and *D*) relate the inlet pressure (p_i) and velocity (v_i) to respective outlet values (p_o, v_o), assuming a plane wave propagation, as expressed in the following equation:

$$\begin{bmatrix} p_i \\ v_i \end{bmatrix} = \begin{bmatrix} A & B \\ C & D \end{bmatrix} \begin{bmatrix} p_0 \\ v_0 \end{bmatrix} \tag{3}$$

Two methods are available to calculate the four-pole parameters, exploiting the transfer-matrix approach: the two-sources and the two-loads methods [22]. When using the two-loads method, four microphones are needed, and the impedance of the termination has to be changed, as shown in Fig. 2. The silencer *TL* can be calculated as follows [22,39]:

$$TL = 20\log_{10}\left\{\frac{1}{2}\left|A_{23} + \frac{B_{23}}{\rho c} + \rho c C_{23} + D_{23}\right|\right\} + 10\log_{10}\frac{S_i}{S_t} \tag{4}$$

where ρ is the fluid density, c is the speed of sound in the fluid medium and A_{23}, B_{23}, C_{23} and D_{23} are the four-pole parameters between microphones 2 and 3. For the specific expressions of the parameters we refer to [22].

As the anechoic conditions can be easily reproduced numerically, but quite impossible to realize in a real case scenario, the decomposition technique is used in the simulations and the two-load technique is adopted for the experimental measurements in this study.

2.2. Experimental mock-up

A mock-up employed to investigate chemical emission, vibration and noise generated by a marine engine has been mounted in a laboratory of the University of Trieste in the context of project ABE [34].

The mock-up (Fig. 3) is composed of a 4-stroke Genset engine with the characteristics reported in Table 1, mounted on a foundation. It is equipped with a modular exhaust line that allows for testing different components in different configurations. The mock-up is used in this study to measure the *TL* of the DOC; the experimental data are used as a reference for the numerical assessment of *TL* calculated with the combined methodology and for the subsequent acoustic properties' optimization. For the sake of clarity, we point out that the term DOC is employed here to indicate the entire converter (Fig. 4), which contains two metallic honeycombs wash-coated with a "diesel oxidation catalyst" based on Pt- doped-Al_2O_3 formulation. The narrow channel of the monoliths has a sinusoidal shape and a density of 300 cells per square inch.

2.3. Experimental measurements to evaluate the TL of the reference DOC

First, the engine target frequencies have to be evaluated, as the *TL* of exhaust line components has to be optimized in correspondence with those values and, even more important, the transparent frequencies of the *TLs (i.e.*, the local minima of the *TL* curves) must not coincide with the engine frequencies. As a matter of fact, the sound waves propagate unaltered through the component in correspondence with the transparent frequencies, leading to null sound attenuation at the outlet.

The exhaust noise spectrum of engines always contains strong tones associated with the rate of cylinder firings. The lowest tone is the *CFR* (Cylinder Frequency Rate), which is the firing rate for every single cylinder, while the *EFR* (Engine Firing Rate) is generally the strongest tone in the exhaust spectrum. For a 4-stroke engine *CFR* and *EFR* can be expressed in the following form [40]:

$$CFR = \frac{RPM}{120} \tag{5}$$

$$EFR = CFR \cdot N_c \tag{6}$$

where N_c is the number of cylinders. Notice that Equation (6) is valid when the cylinders are out of phase, as in the Genset considered in this study. The higher-order harmonics of *CFR* and *EFR* are obtained by multiplying their values by the number of desired harmonics. In general, harmonics up to the 4th order are considered for *TL* optimization, as higher-order harmonics do not significantly influence the exhaust gas noise [41]. Table 2 reports the analytical *EFR* and *CFR* calculated up to the 4th order for the Genset. Fig. 5 reports the narrow band Sound Pressure Level (*SPL*) measured at the outlet of the engine, highlighting the *CFRs* and *EFRs* up to 4th order. Fig. 5 confirms a very good agreement between analytical and experimental frequencies at which *CFRs* and *EFRs* engine harmonics occur.

In this paper, the mock-up is used to measure the *TL* of a DOC and the flow conditions at the inlet and the outlet. Flow conditions are needed to

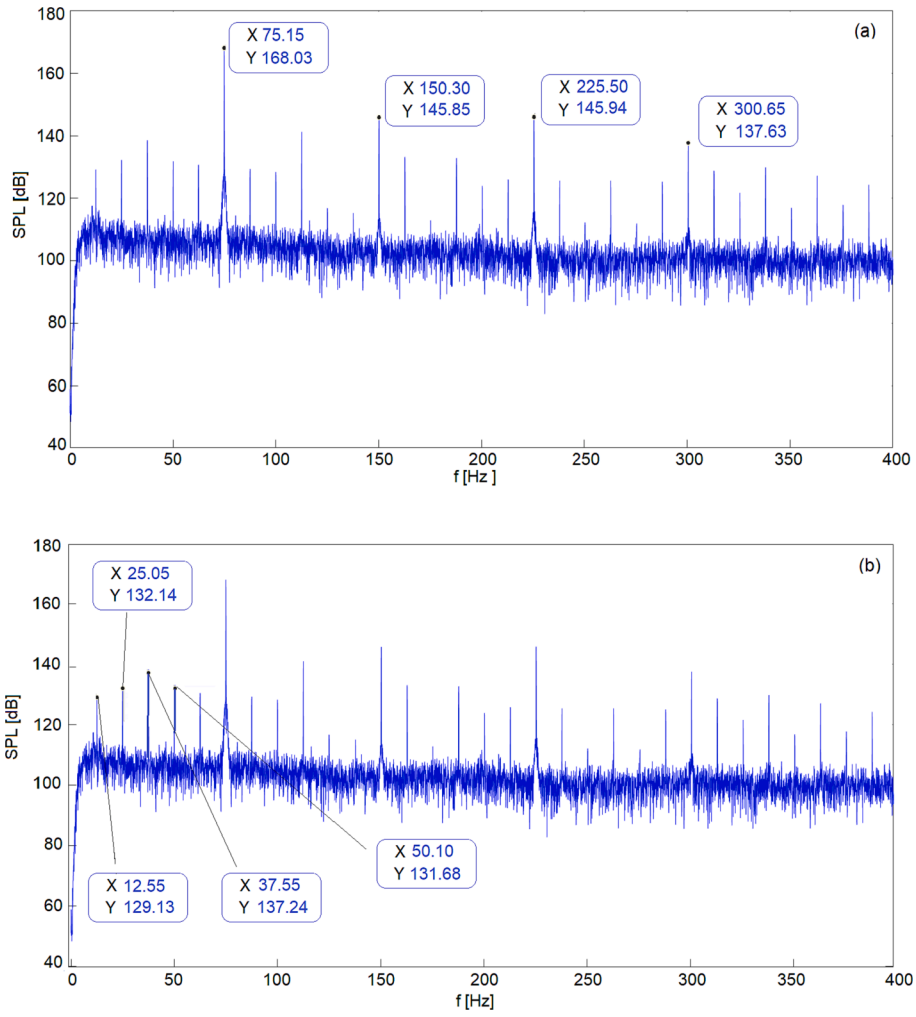

Fig. 5. Narrow band sound pressure level: a) experimental *EFRs* highlighted, b) experimental *CFRs* highlighted.

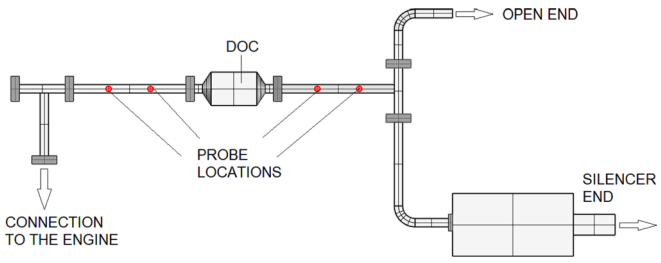

Fig. 6. Configuration of exhaust line for the two-load technique.

Table 3
Experimental average flow conditions.

Configuration	Location	Temperature [°C]	Velocity [m/s]	Relative Pressure [Pa]
Silencer-end	Inlet	269.0 ± 7.0	44.2 ± 9.4	1270 ± 0.6
	Outlet	272.8 ± 4.0	42.8 ± 7.9	710 ± 0.2
Open-end	Inlet	264.7 ± 3.0	44.8 ± 8.3	1280 ± 1.3
	Outlet	270.4 ± 8.3	43.6 ± 4.7	798 ± 1.6

properly elaborate the registered signals to calculate the *TL*, as well as for CFD modelling settings and comparison (see Section 3).

The *TL* is obtained applying the two-loads techniques, using as loads the open-end and the standard silencer of the Genset (Fig. 6). Four microphone locations are considered, two before and two after the DOC (Fig. 6), with a spacing of 300 mm and a distance from the flanges of 5 diameters of the exhaust pipe [42]. The microphone spacing is selected based on the maximum considered frequency [43] that, in this case, is 350 Hz (the 4th order of the *EFR* is at 300 Hz), while the distance from flanges and pipe variation (*e.g.*, section or direction) is considered to avoid flow turbulence, obtaining a flow regime with an almost homogeneous radial velocity distribution [42]. No additional probes to improve the quality of the measure are needed since the flowrate is <0.3 Mach (102 m/s) [44]. GRAS 40SC CCP Probe Microphones are used for the test and the measurement is repeated for three times to ensure its accuracy. The acquired measures are then processed with a Matlab script to obtain the *TL* values as a function of frequency [38].

Flow characteristics are measured with a TCR Tecora Flowtest ST, using a Pitot tube Type L equipped with an S terminal and K thermocouple. The probe is inserted in the same locations as microphones, to such a depth as to measure at the centre of the exhaust pipe. Three measurements, each averaged over 5 min, are performed in every point and the results are reported in Table 3. The relative pressure is calculated considering the ambient pressure as reference one. The experiments are carried out at 80% engine power, conditions typical for a cruising ship.

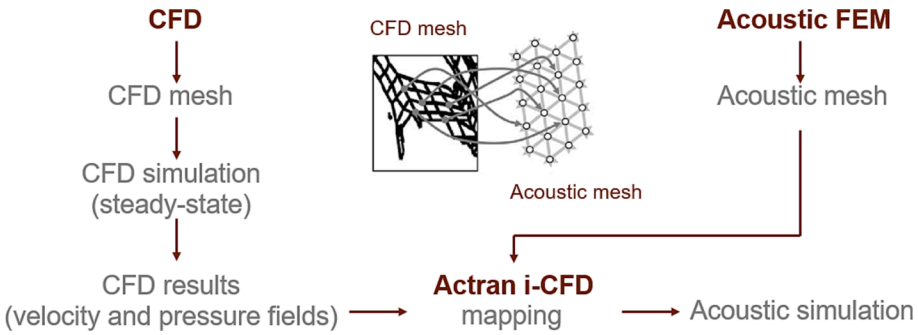

Fig. 7. Workflow of the combined CFD-FEM methodology.

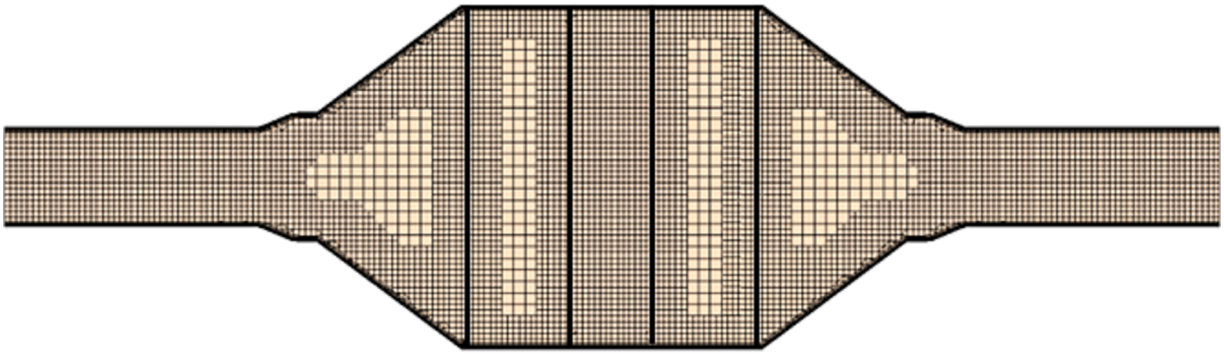

Fig. 8. CFD mesh employed for DOC discretization.

3. The combined CFD-FEM methodology to evaluate the *TL* in the presence of flow

The combined approach proposed in this paper aims to combine the advantages of CFD and FEM approaches to obtain an efficient and accurate methodology able to predict the acoustic properties of exhaust line components. Two fundamental advantages derive from the use of this methodology. First, the acoustic properties, such as *TL*, of a component can be easily calculated with the acoustic FEM model, provided that a reliable flow field is calculated with the CFD model. Second, there is no need for unsteady CFD simulations to properly evaluate the *TL* in the presence of the flow. In fact, a steady-state simulation, which computes the flow field, is sufficient to obtain reliable results, with a significant benefit in terms of total computational effort. In addition, the noise generated by the flow can be evaluated by performing just a simple steady simulation; the Stochastic Noise Generation and Radiation (SNGR) [45] method allows for building unsteady turbulence from mean flow parameters (*e.g.,* turbulent kinetic energy, dissipation and mean velocity field) extracted from a steady CFD simulation. Those parameters are then used to calculate the noise sources using Lighthill [46] and Möhring [47] analogies. Fig. 7 describes the workflow employed.

The flow field and related properties are first calculated using the steady-state CFD. These calculated data are then transferred from the CFD mesh to the acoustic FEM one by using mesh mapping available in the Actran i-CFD tool [48]. This procedure involves two steps: first, the nodes of the CFD mesh are projected on the acoustic mesh, and then the projected values are interpolated and mapped on the FEM mesh nodes based on the shape functions. Note that the CFD mesh has to be finer than the FEM one to avoid loss of information.

Preliminary studies have assessed the CFD [31,48] and FEM [50] results and defined the influence of both mesh topology and simplified methodology to model perforated and narrow channel components. The assessed CFD and FEM simulations are used here for the combined approach to model the acoustic properties of the DOC, mounted along the exhaust line of the Genset mock-up (Fig. 3).

3.1. CFD simulations settings

The CFD simulations are performed using the software Simcenter STAR-CCM+ 2020. RANS (Reynolds Averaged Navier Stokes) equations are used to model the flow, setting the k-ε turbulence model and using it as the working medium air, which is considered as compressible gas with physical properties dependent on the temperature [51]. Notice that the average molecular weight of air is negligibly different from that of diesel engine exhaust. The segregated approach is used, adopting the SIMPLE (Semi Implicit Method for Pressure Linked Equation) algorithm. The prism layer settings are chosen to target a Wall y+ $\leq$ 1, and a trimmed mesh (Fig. 8) is used. Considering that the calculated flow field will be imported in the FEM solver for the evaluation of acoustic properties in the frequency domain, the base size (*bs*) is set according to the following equation:

$$bs = \frac{c}{4f_{max}} \tag{7}$$

where c is the speed of sound in the flow medium and f_{max} is the maximum frequency considered in the study. Moreover, in previous studies [31,49] the choice of the base size following the presented criteria is verified through grid independence study. In accordance with the experimental data reported in Table 3, the boundary conditions are set as follows: velocity inlet (42.5 m/s), pressure outlet (101325 Pa, open end to the atmosphere), no-slip condition at walls, fluid temperature of 270 °C, turbulence intensity of 0.01 and turbulence viscosity ratio of 10. Residuals $<10^{-5}$ are chosen as convergence criterion.

The catalytic monoliths inside the DOC converter are modelled using a porous region. The flow resistivity (R), which is a measure of the resistance that a fluid meets when flowing through a porous material related to the viscous interaction forces between the fluid and the solid

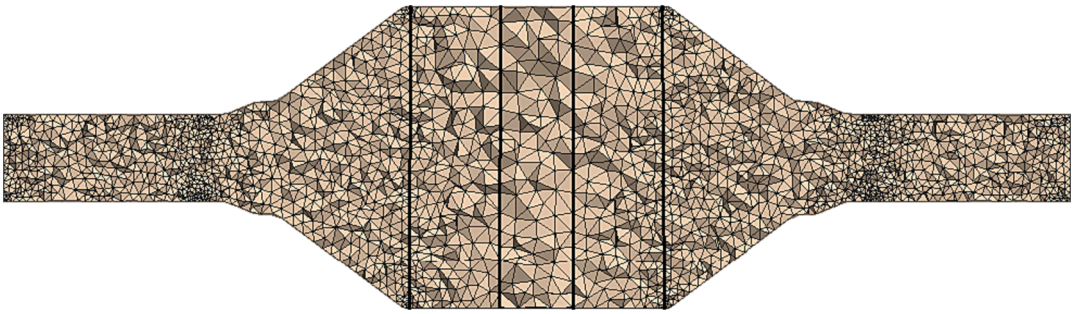

Fig. 9. FEM mesh employed for DOC discretization.

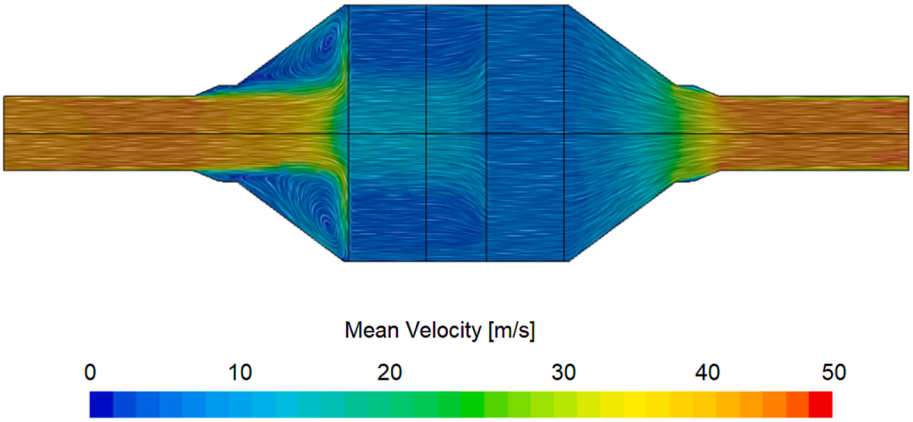

Fig. 10. Velocity flow field with streamlines. Inlet on left side and outlet on right side.

skeleton, is calculated as described in the following text.

Pressure drop (ΔP) in a straight pipe is caused by energy loss due to frictional forces between the flowing medium and the pipe walls and it can be expressed as follows [52]:

$$\Delta P = \varepsilon \frac{L}{D} \frac{1}{2} \rho u^2 \tag{8}$$

where ε is the Darcy friction factor, L is the pipe length, D is the pipe diameter, ρ the fluid density and u is the mean flow velocity. The Darcy friction factor can be derived from the Moody diagram as a function of Reynolds number (Re) and pipe roughness [52]. For laminar flow, as assumed in the narrow channel of the catalytic monoliths, ε can be expressed as follows:

$$\varepsilon = \frac{64}{Re} \tag{9}$$

Combining Eqs. (8) and (9) the Hagen-Poiseuille equation is obtained:

$$\Delta P = \frac{8 \mu h u}{r^2} \tag{10}$$

where h and r are respectively the length and the radius of the pipe and μ is the dynamic viscosity of the flow. The Hagen-Poiseuille equation gives the pressure drop in a fluid flowing through a long cylindrical pipe and can be applied to each cylindrical pipe of a component composed of narrow channels (*e.g.,* catalytic monoliths). The flow resistivity can be related to the pressure drop as follows:

$$R = \frac{\Omega \Delta P}{h u} \tag{11}$$

Combining Eqs. (10) and (11) the following expression can be derived for the flow resistivity in cylindrical narrow channel component:

$$R = \frac{8 \mu \Omega}{r^2} \tag{12}$$

where Ω is the Open Area Ratio (OAR). For channels with different shapes (*e.g.,* sinusoidal) the hydraulic radius r_h can be used:

$$r_h = 4 d_h = \frac{A}{P} \tag{13}$$

where A is the cross-sectional area of the channel and P the wet perimeter.

The catalyst used in this study has an OAR of 0.92 and a hydraulic diameter of a channel equal to $0.62 \cdot 10^{-3}$ m, leading to a flow resistivity of 678 N·s/m^4 at 270 °C (exhaust gas temperature).

3.2. FEM simulations settings

The software Actran VI 2020 is used in this study for the acoustic FEM simulations. A Direct Frequency Response (DFR) analysis is performed, and the geometry is discretized using a tetrahedral mesh (Fig. 9) with 10 linear elements per wavelength [50,53]. Such modelling is different from the one employed by the CFD solver for viscous flow simulations (Fig. 8): for CFD simulations a trimmed mesh is used to reach a computationally-efficient and accurate solution [54], a prism layer is considered to solve the boundary layer due to the fluid flowing along the surfaces [55] and refinement blocks are set at the inlet and at the outlet of the monoliths to better capture local phenomena in these regions. For acoustic-FEM simulations, the use of tetrahedral mesh is advised with the need of at least 10 linear elements per wavelength, considering the maximum analysed frequency [48,56]; no refinement areas or prism layers are needed.

As for the adopted boundary conditions, at the inlet, the duct modes [50] are used to model the incident acoustic wave, imposing a plane

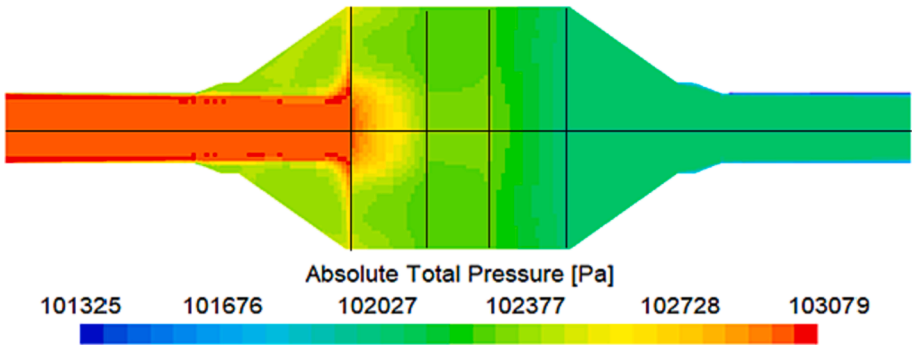

Fig. 11. Absolute total pressure flow field. Inlet on left side and outlet on right side.

Table 4
Calculated values and the differences (%) with respect to the experimental values obtained at the inlet and at the outlet of the modelled DOC. Average values are reported.

Location	Temperature [°C]	Temperature Difference (%)	Velocity [m/s]	Velocity Difference (%)	Relative Pressure [Pa][a]	Relative Pressure Difference (%)
Inlet	269.9	0.3	45.1	2	1314	3.4
Outlet	268.5	1.5	43.9	2.5	738	3.9

[a] The relative pressure is calculated considering the ambient pressure as the reference one.

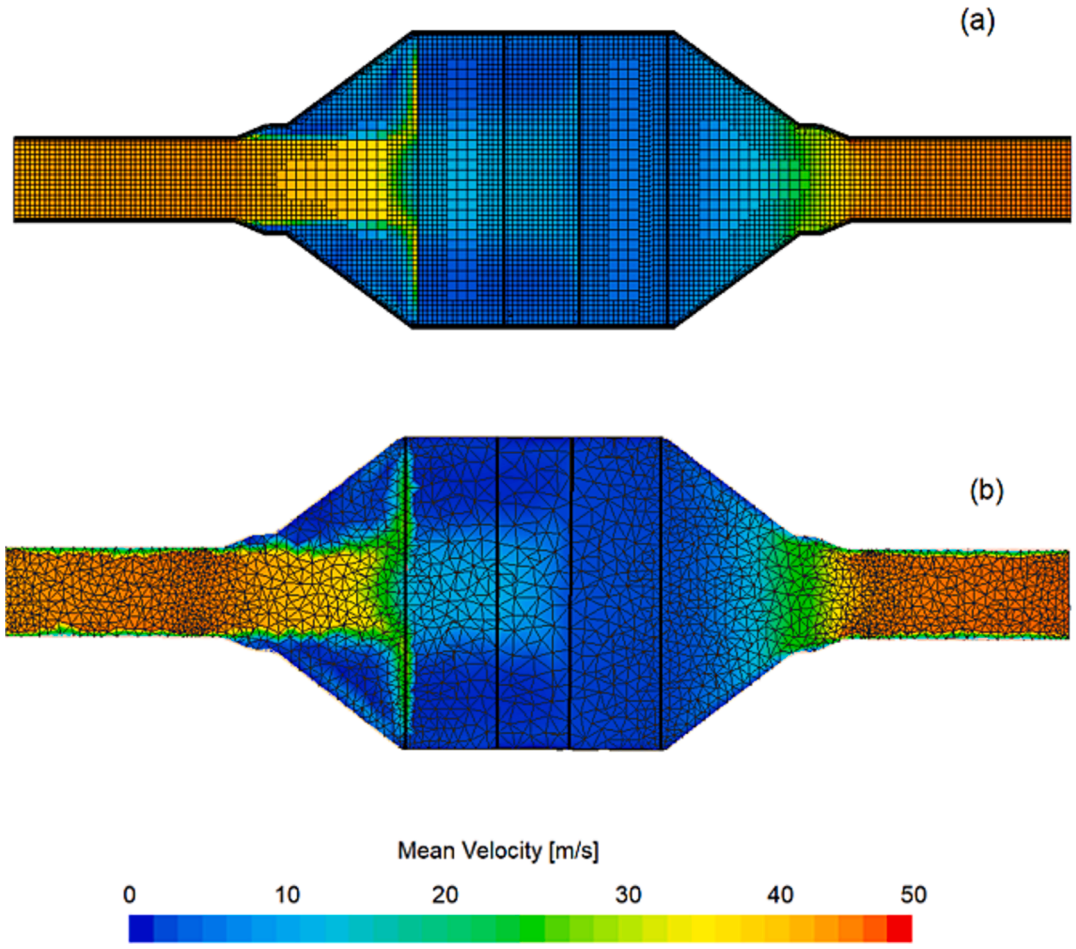

Fig. 12. Velocity flow field: (a) CFD vs (b) imported FEM. Inlet on left side and outlet on right side.

wave propagation in a frequency range of 0–650 Hz. To avoid reflection, free mode propagation is set in the direction opposite to the excitation. At the outlet, the anechoic condition is modelled using the duct modes and by setting free mode propagation.

The catalysts inside the DOC are modelled using visco-thermal components: visco-thermal effects appear when sound waves travel through thin air layers or narrow channels and dissipation occurs due to the boundary layer created by the viscosity.

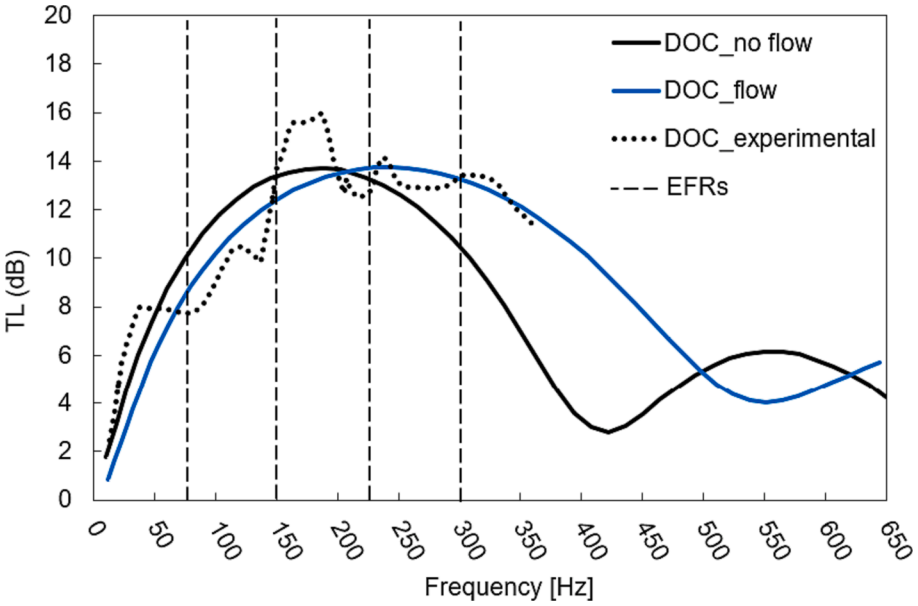

Fig. 13. Comparison of numerical *TL* with and without flow.

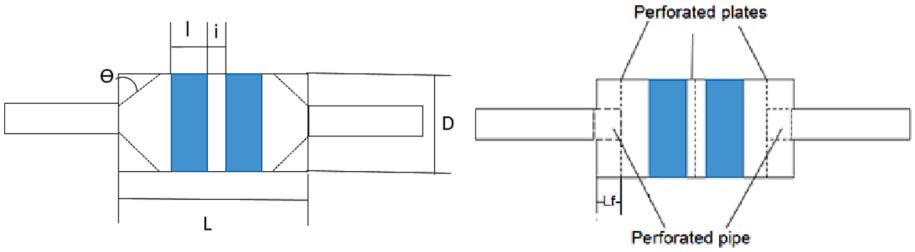

Fig. 14. Identification of predictor parameters.

Table 5
Predictor variables and their limits.

	D [mm]	Θ [deg]	L [mm]	l [mm]	i [mm]	D_f [mm]	R [N·s/m^3]	OAR [-]	L_f [mm]	n_p [-]
Max	598	45	1020	180	120	35	678	0.98	Lc/2	3
Min	297	0	510	90	60	10	520	0.92	0	0

Table 6
Optimum solution vs reference parameters.

	D [mm]	Θ [deg]	L [mm]	l [mm]	i [mm]	R [N·s/m^3]	OAR [-]	L_f [mm]	n_p [-]
Reference	297	40	510	90	60	678	0.92	0	0
Optimized	594	0	1020	180	60	678	0.92	0	0

The use of such component requires the knowledge of the fluid characteristics (*i.e.,* temperature and velocity), the OAR of the component and the channel shape (*e.g.,* hydraulic radius for sinusoidal channel). This approach involves reduction of the full Linearized Navier-Stokes-Fourier (LNSF) equations into an equivalent fluid scalar equation involving only the acoustic pressure (also called equivalent fluid equations). Actran implements the Low Reduced Frequency (LRF) model developed by Beltman [57], with the extension proposed by Sambuc et al. [58], which handles the presence of a mean flow inside the fluid domain within waveguide geometries (*e.g.,* thin layer and narrow channel). The final equivalent fluid model is obtained from the continuity equation of LNSF by substitution of the state equation, the thermal and the shear velocity solutions. The pressure wave equation is integrated over the cross-section and leads to the following 1D dissipative convective wave equation [59]:

$$\nabla_{pd}\left(H\nabla_{pd}p'\right) - \widehat{M_0^2}\gamma N^{-1}\nabla_{pd}^2 p' - 2ik_0\gamma N^{-1}\widehat{M_0}\nabla_{pd}p' + k_0^2\gamma N^{-1}p' = ik_0R \qquad (14)$$

where $\widehat{M_0}$ is the mean Mach number, R the source term derived from the velocity along the cross-sectional direction, γ the ratio of specific heats, ∇_{pd} the gradient along the propagation direction and p' the acoustic perturbation of pressure.

This wave equation is a generalization of the conventional convective Helmholtz equation which introduces thermo-viscous dissipation through the complex parameters H and N (dimensionless factors corresponding to corrective terms for the density and the bulk modulus, respectively).

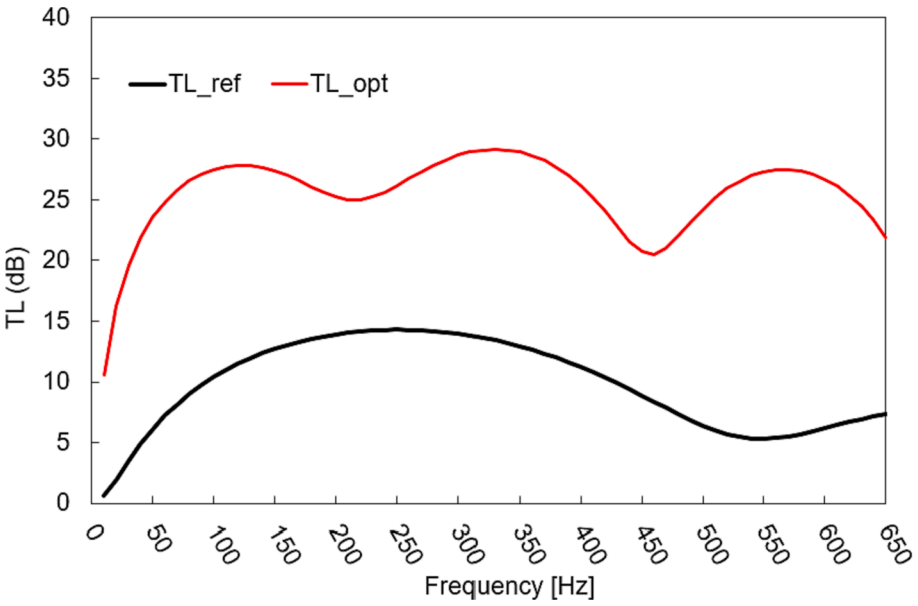

Fig. 15. Comparison between optimized and reference TL.

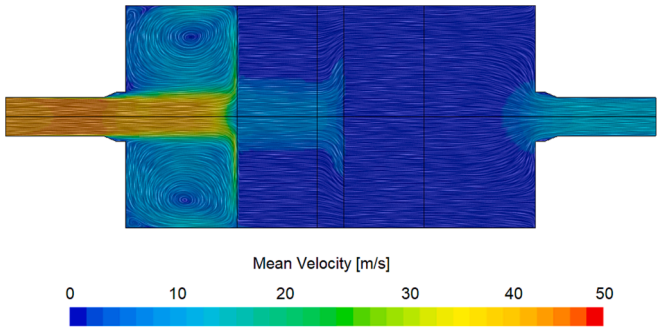

Fig. 16. Velocity field with streamlines in the optimized DOC. Inlet on left side and outlet on right side.

3.3. Numerical results

As previously explained, the first step of the numerical method is the calculation of the flow field with a CFD simulation. Fig. 10 and Fig. 11 report the obtained velocity and the pressure fields, while Table 4 reports temperature, velocity and relative pressure values calculated in the same location of the probe used in the experimental measurements (Fig. 6). The comparison with the experimental values is also reported in Table 4, As above mentioned, the relative pressure is calculated considering the ambient pressure as reference one. Considering the experimental measurement errors (compare the standard deviation in Table 3) was caused by both the sensitivity of the instrumentation used and the difficulties of the measurement itself (*e.g.*, difficulty in positioning the probe due to the high temperatures of the pipeline, disturbed flow due to elbows and joints), a discrepancy between numerical and experimental data <5% is considered as a good matching between experiment and numerical results.

Importantly, both the experimental measurements and the numerical simulation show that the back pressure generated by the DOC (1458 Pa) is well below the maximum allowable Genset back pressure of 4900 Pa; accordingly, no negative influence on the engine efficiency is expected.

In order to numerically evaluate the *TL* of the DOC, the flow field calculated with the CFD is transferred onto the FEM mesh through mesh mapping (Fig. 7). Fig. 12 shows the effectiveness of this procedure: the velocity field calculated on the CFD mesh with Star-CCM+ (Fig. 12a) well compares the one imported onto the acoustic-FEM mesh in Actran VI (Fig. 12b).

Fig. 13 compares the experimental *TL* values with those calculated by FEM (no flow) and the CFD-FEM methodology (with flow). The presence of the flow (*i.e.*, temperature and velocity) shifts the maximum of *TL* curves towards higher frequencies and it well correlates with the experimental measurement performed on the diesel Genset mock-up. This clearly illustrates the efficiency of the present computational methodology: all the calculations could be performed on a common notebook equipped with an Intel core I7 processor.

The observed maximum discrepancy between the CFD-FEM *TL* and experimental curves of 2 dB is a notably good data correlation, considering that the experimental measurements can be influenced by flow fluctuations, besides the other critical issues of the measurements (*e.g.*, sensitivity of microphones, their positioning with respect to the diameter of the pipe, flow turbulence).

4. Acoustic performances of the integrated abatement system

4.1. Optimization of the contribution of DOC

The Response Surface Methodology (RSM) [60] is used to build a surrogate model (metamodel) that allows fast evaluation of *TL* curve to be employed in the optimization process of the silencing properties of the DOC. The use of RSM involves the following fundamental steps: i) design a series of experiments for adequate and reliable measurement of the analysed response; ii) creation of a mathematical model that fits the real-valued response; iii) analysis of optimum operating conditions.

Design of Experiment (DoE) can be used to create the database of *TL* values as a function of predetermined parameters needed to construct the metamodel. The predictor parameters with their constraints constitute the design space.

In the presented study, the following characteristics have been selected as predictor variables (Fig. 14): length of the DOC (L), angle of the conical expansion (Θ), length of the catalytic monoliths (l), length of the interstice between the monoliths (i), DOC diameter (D), length of the perforated pipe at the inlet/outlet (l_f), the number of added perforated plates (n_p), the diameter of the holes in the perforated plates (D_f), flow resistivity of the catalysts (R), OAR of catalysts. Table 5 the reports both upper and lower limits for each variable; these limits are established on the basis of chemical considerations and they represent constraints in

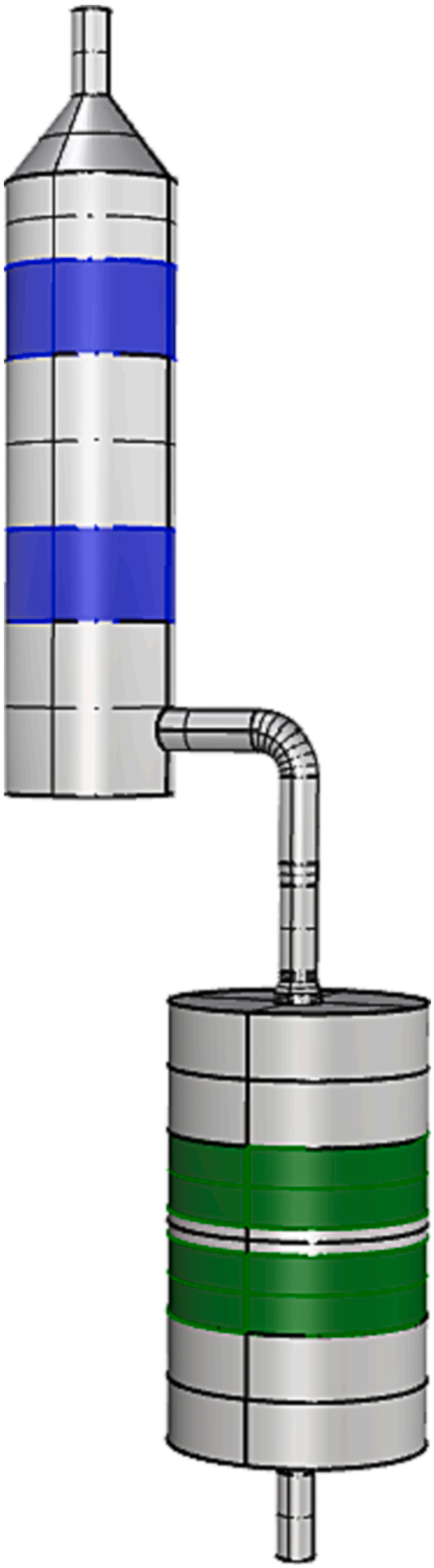

Fig. 17. Layout of the exhaust line with DOC and scrubber in series.

the sense that any variation must not decrease the catalytic efficiency of the DOC. As a matter of fact, to ensure an efficient NOx conversion, a series of parameters must be controlled and respected; for example, the contact time between exhaust gas and catalysts or adequate cell dimensions to avoid clogging due to particulate matter in the exhaust [12].

The adoption of simple fractional design methods or derived ones (*e.g.,* central composite designs or Box-Behnken methods [61]) for the DoE determination of the simulation scenario is not advisable due to the complexity of possible mutual interactions of design parameters on predicted *TL* values. To this end, an alternative strategy has been used for the *TL* database creation, *i.e.*, the adoption of a Stratified Latin Hypercube Algorithm [62].

Once a *TL* database is generated employing multiple calculations with the proposed combined FEM-CFD numerical methodology for each case found through DoE, a multiple linear regression is used as mathematical surrogate model for *TL* prediction. In this study, regressions are performed using a stepwise selection process [63]. Regressions on *TL* values pertain to specific frequencies from 50 to 400 Hz in steps of 50 Hz. The stepwise process automatically selects the predictor variables significant to the model discarding the non-significant terms through the evaluation of *p*-values (if $p < 0.001$ then the term is removed).

A Genetic Algorithm (GA) [64] is then used to evaluate the optimum combination of parameters that ensure the *TL* maximization of the DOC in the prescribed frequency range. The optimization procedure is implemented with a Matlab script, an Augmented Lagrangian Genetic Algorithm (ALGA) [65] is applied to solve nonlinear constraint problems. In the presented case, the optimization process aims at maximizing the *TL* in the frequency range of interest. To this end, the area under the *TL* curve (*A*) is selected as representative objective function of the stated problem, with the additional nonlinear constraint $(c_i(x))$ that the *TL* cannot be <25 dB (TL_{min}). So, the optimization problem can be expressed by the following equations:

$$\min_x(f(x)) \tag{15}$$

$$f(x) = -A \tag{16}$$

such that:

$$c_i(x) \leq 0 \tag{17}$$

$$c_i(x) = -TL(x) - TL_{min} \tag{18}$$

It is important to point out that the negative value of the area under the *TL* curve is selected as objective function since the ALGA finds the minimum of the function.

The frequency range of interest is that from 10 to 400 Hz, *i.e.,* frequencies where the highest engine noise is perceived (Fig. 5). The marine silencer typically ensures a sound abatement of about 30–35 dB. A limit of 25 dB as a minimum noise abatement efficiency for the *TL* of the DOC is chosen here, since, in the real case scenario, DOC is mounted in series with the scrubber; accordingly, the abatement of 30–35 dB has to be ensured by the whole system. Setting higher limits for the DOC would result in over dimensioning of the whole system.

The optimized geometrical parameters are reported in Table 6 and compared with the dimension of the reference DOC. Fig. 15 reports the comparison between the reference *TL* of the standard DOC and the optimized *TL* and it highlights an increase of the *TL* of about 25 dB with a minimum of 20 dB at 450 Hz, which is, however, outside the frequency range of interest. The optimization leads to an increase of the dimensions of the converter, yet a significant volume savings of approximately 45% is achieved if compared to an equivalent system consisting of a DOC coupled to a silencer.

As a result of the increased volume, the velocity field calculated with the CFD solver (Fig. 16) shows significantly different profile in the optimized DOC with respect to the reference DOC: the central cylindrical

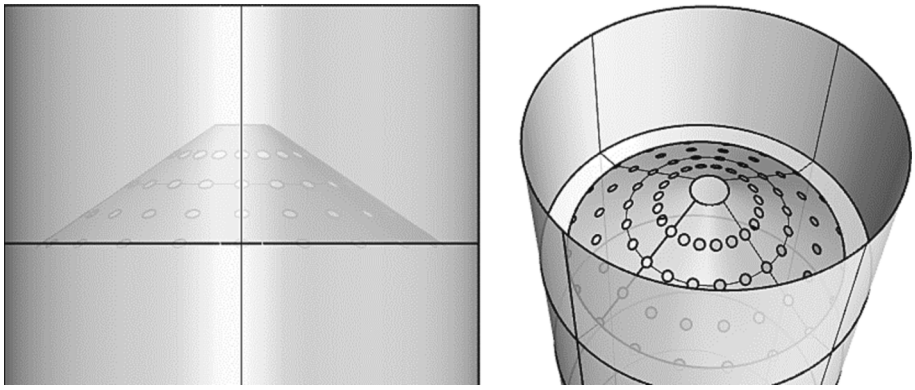

Fig. 18. Particular of the perforated cone inside the scrubber.

Table 7
Geometrical parameters of the tower packing model scrubber.

D inlet/outlet [mm]	88.9
D chamber [mm]	202
L inlet/outlet [mm]	100
L chamber [mm]	1090
H inlet [mm]	150
H conical adapter [mm]	100
Distance between fillers [mm]	200
H first filler [mm]	250
R [N·s/m^3]	520
OAR [-]	0.98
H perforated steel cone [mm]	150
d perforations [mm]	10
holes spacing [mm]	15
Thickness [mm]	3

zone of higher velocity along the first catalytical monolith in the optimized DOC features an average velocity of 8 m/s, which decreases to 3 m/s in the lower velocity regions within both the catalytic monoliths. In the reference DOC the higher velocity region shows an averaged values of 15 m/s and lower velocity regions of 4 m/s and 7 m/s respectively in the first and in the second monolith. Moreover, in the first part of the converter, before the first monolith, a significant turbulence is found that would homogenise the exhaust mixture before entering the monolith. The different velocity patterns which increase the contact time of the exhausts with the catalyst, and the pre-mixing of the exhaust, should increase the chemical efficiency, which is clearly a desirable output as the high conversion of NO to NO_2 is critical for NOx removal [17].

4.2. *Acoustic performances of the optimized DOC – Scrubber system*

The overall acoustic performance of the exhaust line is simulated by considering the optimized DOC located prior to a model-scale tower packing scrubber (Fig. 17). To improve the *TL* of the scrubber, two perforated steel sheets with conical shape (Fig. 18) are inserted under each packing stage. In Table 7 the geometrical parameters of the tower packing scrubber are summarized.

The *TL* curves of the single components and that of the whole apparatus are reported in Fig. 19. A *TL* up to 50 dB with minima above 30 dB is ensured in the whole frequency range of interest. Also important is that the minima of the *TL* do not coincide with the *EFRs*: a *TL* of 35 dB is observed at 225 Hz corresponding to the 3rd harmonics, where the silencing effect is least efficient. As previously mentioned, to reduce the exhaust gas noise, the transparent frequencies must not coincide with the engine frequencies. Notice that the *TL* calculated for the integrated system is obviously not a simple sum of the single contribution indicating that there is room for further improvement of the *TL* by considering the mutual acoustic interactions of the two devices. Moreover, should be consideredthe obtained *TL* is a function of the considered flow conditions, *i.e.*, velocity and temperature, as underlined in Fig. 13.

Recalling that the sound attenuation of marine silencers is about 30–35 dB, the obtained result in terms of *TL* indicates that the elimination of the silencer from the Genset exhaust line is well-feasible for the set-up adopted in this study. Such results save space- on board, allowing an easier installation of emission control devices (*i.e.,* DOC and scrubber). Notably, such a configuration of exhaust line, in principle accomplishes both noise and chemical emissions (*i.e.,* PM, HC, SOx and

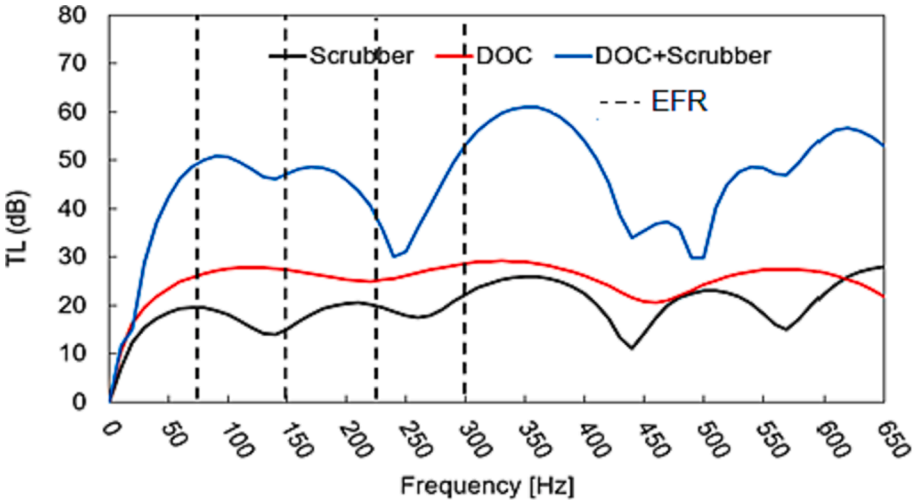

Fig. 19. *TL* of the exhaust line component, in series and alone. Highlighted are the *EFR* and its harmonics.

NOx), without the need for installation of other components such as SCR or EGR. Furthermore, such an exhaust line configuration generates a back pressure of 4510 Pa, which is less than the maximum allowable back pressure for the Genset (4900 Pa).

The combined CFD-FEM approach here described presents some limits due to the adoption of simplified models such as steady state CFD simulations for the evaluation of flow field and the strategies to model internal components without the need to design and mesh their exact geometry (*e.g.*, porous region and viscous-thermal component). Moreover, parameters such as surface roughness, which in the real case scenario influences the performances of the after-treatment systems, or the water spray inside the scrubber are not considered. On the contrary, the methodology does not require the knowledge of parameters difficult to estimate with measurements, while it allows to have a methodology capable of predict the acoustic properties of after-treatment system, study their integration and optimize their performances and volumes, already in an early design stage. Of paramount importance, especially for the application in industrial sectors, is that the proposed methodology has a low computational effort,

To extend the applicability of this methodology to the industry, the optimization process should be applied to the whole system *(i.e.*, DOC plus real scrubber) to further optimize the design, volumes and operation conditions. Moreover, the influence of water spry inside the scrubber on the acoustic properties should be evaluated. As for the noise generated by the exhaust gas itself, preliminary simulations using SNGR suggest that the noise generated by flow turbulence is limited to high frequencies and tends to be a local phenomenon (*i.e.*, not carried by the gases up to the exit of the funnel and radiated to the outside). Further investigation should be performed to properly assess this aspect.

We advise that the methodology is applied here to a high-speed diesel engine, yet we believe that the proposed methodology can be easily extended also to the medium-speed diesel engines, typically installed onboard, since such marine after-treatments systems have comparable both geometry and limitations in terms of performances. The differences are represented by the overall volumes of the real after-treatments systems and by different conditions of the gas flow, *i.e.*, temperature and velocity, that influence the *TL*, as already mentioned in the paper. However, all these parameters can be modified and inserted in the optimization process without the need to modify the workflow.

5. Conclusions

As shown in this work, CFD, FEM simulations and GA optimization represent an effective calculation framework capable of properly model and optimize the acoustic properties of exhaust line components coupled to a marine diesel engine. The proposed methodology is able to provide solutions for the design of marine engine exhaust systems, combining several after-treatment devices and focusing on reducing the exhaust gas noise and minimizing the exhaust gas system volume, without reducing the efficiency of the chemical pollution abatement (*e.g.,* SOx and NOx).

The novel combined CFD-FEM methodology provides reliable results under realistic conditions as it considers the influence of the exhaust flow while reducing the computational effort. The reliability of the methodology has been assessed using either literature data or experimental measurements and by considering the influence of several parameters such as mesh typology and dimensions, different approaches to model porous, perforated and narrow channel components, different aspects of energy dissipation inside such devices [32,49,50,66].

The CFD-FEM methodology is applied here to an industrially relevant system such as DOC and scrubber: it allows to properly model the acoustic properties (*i.e.*, *TL*), the generated backpressure and the velocity/pressure field inside the components.

Successful application of the *ad-hoc* GA optimization to the DOC leading to a combination of geometrical parameters that maximizes its *TL*, predicts that use of the optimized DOC, in series with a model-scale tower packing scrubber, allows to exclude the silencer from the Genset exhaust line.

We believe that application of the proposed tools in the maritime industry is straightforward for the design of marine exhaust lines already in the early stage of the design phase, thanks to the low computational efforts and relatively easy usage, since reliable results were obtained on an industrially relevant prototype, despite the simplifications employed. Extension of these methodologies to other fields/applications would certainly be of strong interest.

CRediT authorship contribution statement

Giada Kyaw Oo D'Amore: Conceptualization, Methodology, Validation, Software, Data curation, Writing – original draft, Writing – review & editing. **Mitja Morgut:** Supervision, Writing – review & editing, Software. **Marco Biot:** Funding acquisition, Supervision, Writing – review & editing. **Francesco Mauro:** Conceptualization, Methodology, Supervision, Writing – review & editing, Data curation, Validation, Software. **Jan Kašpar:** Conceptualization, Funding acquisition, Supervision, Writing – review & editing.

Declaration of Competing Interest

The authors declare that they have no known competing financial interests or personal relationships that could have appeared to influence the work reported in this paper.

Data availability

All the data used in the study are reported or referenced in the text

Acknowledgements

The authors wish to gratefully thank Carlo Pestelli and Marko Gantar from Wärtsilä Italy S.p.A. for their helpful discussions and their valuable assistance in the experimental tests.

Funding

This work was supported by the "ABE-Abbattimento delle emissioni vibroacustiche e chimiche in ambito navale" project funded by Regione Autonoma Friuli Venezia Giulia, POR-FESR 2014–2020, attività 1.3b Incentivi per progetti di R&S da realizzare attraverso partenariati pubblico privati nelle aree di specializzazione Tecnologie Marittime e Smart Health—DGR 849/16.

References

[1] Adam AF, Moldovan IAG, Nita SC, Hrebenciuc A. The Importance of Maritime Transport for Economic Growth in the European Union: A Panel Data Analysis. Sustainability 2021;13:7961. https://doi.org/10.3390/su13147961.
[2] https://www.emsa.europa.eu/tackling-air-emissions/air-pollutants.html (accessed May 16, 2023).
[3] IMO. Revised MARPOL Annex VI. 2008.
[4] Chen Y, Lv L. Design and evaluation of an Integrated SCR and exhaust Muffler from marine diesels. Journal of Marine Science and Technology 2015;20:505–19. https://doi.org/10.1007/s00773-014-0302-1.
[5] Ushakov S, Stenersen D, Einang PM, Ask TØ. Meeting future emission regulation at sea by combining low-pressure EGR and seawater scrubbing. Journal of Marine Science and Technology (Japan) 2020;25:482–97. https://doi.org/10.1007/s00773-019-00655-y.
[6] Zhao Y, Fan Y, Fagerholt K, Zhou J. Reducing sulfur and nitrogen emissions in shipping economically. Transportation Research Part D: Transport and Environment 2021;90:102641. https://doi.org/10.1016/j.trd.2020.102641.
[7] Jang J, Na S, Roh H, Ahn S, Choi G. Spraying and Mixing Characteristics of Urea in a Static Mixer Applied Marine SCR System. Energies 2021;14:5788. https://doi.org/10.3390/en14185788.
[8] Konstandopoulos AG, Zarvalis D, Chasapidis L, Deloglou D, Vlachos N, Kotrba A, et al. Investigation of SCR Catalysts for Marine Diesel Applications. SAE International Journal of Engines 2017;10(4):1653–66.
[9] https://shipandbunker.com/prices/emea/nwe/nl-rtm-rotterdam#IFO380 2023 (accessed May 15, 2023).

[10] Lindstad HE, Rehn CF, Eskeland GS. Sulphur abatement globally in maritime shipping. Transportation Research Part D: Transport and Environment 2017;57:303–13. https://doi.org/10.1016/j.trd.2017.09.028.
[11] https://www.wartsila.com/media/news/22-09-2020-scrubbers-shown-to-have-lower-climate-impact-than-low-sulphur-fuel-2786812 2020 (accessed May 6, 2023).
[12] IMO. RESOLUTION MSC.337(91), CODE ON NOISE LEVELS ON BOARD SHIPS. 2012.
[13] Loyd's Register. Procedure for the Determination of Airborne Noise Emissions from Marine Vessels. 2019.
[14] European Committee for Standardization. Directive 2006/87 - 2006/87/EC Directive of the European Parliament and of the Council of 12 December 2006 laying down technical requirements for inland waterway vessels. 2006.
[15] Liu C, Cao Y, Liu Y, Zhang W, Zhang X, Ming P. Analysis of Intake Silencer Insertion Loss in a Marine Diesel Engine Turbocharger Based on Computational Fluid Dynamics and Acoustic Finite Element Method. Journal of Engineering for Gas Turbines and Power 2019;141:091012. https://doi.org/10.1115/1.4043966.
[16] Bodn H, Glav R. Exhaust and Intake Noise and Acoustical Design of Mufflers and Silencers. In: Crocker MJ, editor. Handbook of Noise and Vibration Control, Hoboken, NJ, USA: John Wiley & Sons, Inc. 2007. 1034–53. doi: 10.1002/9780470209707.ch85.
[17] Boscarato I, Hickey N, Kašpar J, Prati MV, Mariani A. Green shipping: Marine engine pollution abatement using a combined catalyst/seawater scrubber system. 1. Effect of catalyst. Journal of Catalysis 2015;328:248–57. https://doi.org/10.1016/j.jcat.2014.12.013.
[18] Wartsila Corporation. https://cdn.wartsila.com/docs/default-source/product-files/egc/brochure-o-env-wartsila-nox-reducer.pdf 2022 (accessed April 15, 2023).
[19] Denia FD, Martínez-Casas J, Carballeira J, Nadal E, Fuenmayor FJ. Computational performance of analytical methods for the acoustic modelling of automotive exhaust devices incorporating monoliths. Journal of Computational and Applied Mathematics 2018;330:995–1006. https://doi.org/10.1016/j.cam.2017.03.010.
[20] Ryu M-R, Park K. Analysis of Composite Scrubber with Built-In Silencer for Marine Engines. J Mar Sci Eng 2021;9:962. https://doi.org/10.3390/jmse9090962.
[21] Sridhara BS, Crocker MJ. Review of theoretical and experimental aspects of acoustical modeling of engine exhaust systems. Journal of the Acoustical Society of America. 1994. 95. 2363–70. doi: 10.1121/1.408746.
[22] Tao Z, Seybert AF. A Review of Current Techniques for Measuring Muffler Transmission Loss, SAE International; 2003, p. 2003-01–1653. doi: 10.4271/2003-01-1653.
[23] Selvakumar K, Kim MY. A numerical study on the fluid flow and thermal characteristics inside the scrubber with water injection. Journal of Mechanical Science and Technology 2016;30:915–23. https://doi.org/10.1007/s12206-016-0145-2.
[24] Fan W, Guo L-X. An Investigation of Acoustic Attenuation Performance of Silencers with Mean Flow Based on Three-Dimensional Numerical Simulation. Shock and Vibration 2016;2016:1–12. https://doi.org/10.1155/2016/6797593.
[25] Kalita U, Singh DM. Design and CFD analysis on flow through a Reactive muffler of four-cylinder diesel engine 2020. 13.
[26] Zhang H, Fan W, Guo L-X. A CFD Results-Based Approach to Investigating Acoustic Attenuation Performance and Pressure Loss of Car Perforated Tube Silencers. Applied Sciences 2018;8:545. https://doi.org/10.3390/app8040545.
[27] Jeon S, Kim D, Hong C, Jeong W. Acoustic performance of industrial mufflers with CAE modeling and simulation. International Journal of Naval Architecture and Ocean Engineering 2014;6:935–46. https://doi.org/10.2478/IJNAOE-2013-0223.
[28] Fu J, Xu M, Zheng W, Zhang Z, He Y. Effects of structural parameters on transmission loss of diesel engine muffler and analysis of prominent structural parameters. Applied Acoustics 2021;173:107686. https://doi.org/10.1016/j.apacoust.2020.107686.
[29] Swamy M, Kulkarni R, Dharmadhikari R, Rajput S. Estimation of Pressure Drop across Exhaust System by CFD. SIMULATION 2020;07:7.
[30] Liu L, Zheng X, Hao Z, Qiu Y. A time-domain simulation method to predict insertion loss of a dissipative muffler with exhaust flow. Physics of Fluids. 2021. 33. 067114. doi: 10.1063/5.0056316.
[31] Zhu DD, Ji ZL. Transmission loss prediction of reactive silencers using 3-D time-domain CFD approach and plane wave decomposition technique. Applied Acoustics 2016;112:25–31. https://doi.org/10.1016/j.apacoust.2016.05.004.
[32] Kyaw Oo D'Amore G, Mauro F. Numerical study on modelling perforated elements using porous baffle interface and porous region. JEDT 2021. https://doi.org/10.1108/JEDT-07-2021-0356.
[33] Gardner B, Mejdi A, Musser C, Chaigne S, De Campos Macarios T. Coupled CFD and Vibro-Acoustic Modeling of Complex-Shaped Mufflers Accounting for Non-Uniform Mean Flow Effects, 2015, p. 2015-01–2313. doi: 10.4271/2015-01-2313.
[34] ABE - Abbattimento delle emissioni vibro acustiche e chimiche in ambito navale, project funded by Regione Autonoma Friuli Venezia Giulia, POR-FESR 2014–2020, attività 1.3b Incentivi per progetti di R&S da realizzare attraverso partenariati pubblico privati nelle aree di specializzazione Tecnologie Marittime e Smart Health—DGR 849/16. 2022.
[35] Ayre LS, Johnson DR, Clark NN, England JA, Atkinson RJ, McKain DL, et al. Novel Nox emission reduction technology for diesel marine engines. American Society of Mechanical Engineers, Internal Combustion Engine Division (Publication) ICE 2011:703–10. https://doi.org/10.1115/icef2011-60182.
[36] Chung JY, Blaser DA. Transfer function method of measuring in-duct acoustic properties. II. Experiment. The Journal of the Acoustical Society of America. 1980. 68. 914–21. doi: 10.1121/1.384779.
[37] Chung JY, Blaser DA. Transfer function method of measuring in-duct acoustic properties. I. Theory. The Journal of the Acoustical Society of America. 1980. 68. 907–13. doi: 10.1121/1.384778.
[38] Munjal ML. Acoustics of Ducts and Mufflers. 2nd ed. Chichester, United Kingdom: John Wiley & Sons, Ltd; 2014.
[39] Munjal ML, Doige AG. Theory of a two source-location method for direct experimental evaluation of the four-pole parameters of an acoustic element. Journal of Sound and Vibration 1990;141(2):323–33.
[40] Rao PC, Varma BM. Muffler Design, Development and Validation. Methods 2007;5:14.
[41] Shah S, Kuppili S, Hatti K, Thombare D. A Practical Approach towards Muffler Design, Development and Prototype Validation, 2010, p. 2010-32–0021. doi: 10.4271/2010-32-0021.
[42] EN ISO 16911-1: Stationary source emissions - Manual and automatic determination of velocity and volume flow rate in ducts - Part 1: Manual reference method. 2013.
[43] ISO. 10534-2- Determination of sound absorption coefficient and impedance in impedances tubes - Part 2: Transfer function method. 2001.
[44] Jang S-H, Ih J-G. On the multiple microphone method for measuring in-duct acoustic properties in the presence of mean flow. The Journal of the Acoustical Society of America. 1998. 103. 1520–6. doi: 10.1121/1.421289.
[45] Bailly C, Juve D. A stochastic approach to compute subsonic noise using linearized Euler's equations. 5th AIAA/CEAS Aeroacoustics Conference and Exhibit, Bellevue, WA, U.S.A.: American Institute of Aeronautics and Astronautics. 1999. doi: 10.2514/6.1999-1872.
[46] M. J. L ighthill. On sound generated aerodynamically I. General theory. 1951. 24.
[47] Mohring W. A well posed acoustic analogy based on a moving acoustic medium. ArXiv:10093766 [Physics] 2010.
[48] Hexagon. Actran 2020 User's Guide. 2020.
[49] Kyaw Oo D'Amore G, Morgut M, Biot M, Mauro F. Numerical study on the influence of porous baffle interface and mesh typology on the silencer flow analysis. Mar Syst Ocean Technol 2022;17(2):71–9.
[50] Kyaw Oo D'Amore G, Biot M, Mauro F, Kašpar J. Green Shipping—Multifunctional Marine Scrubbers for Emission Control: Silencing Effect. Applied Sciences 2021;11(19):9079.
[51] https://www.engineeringtoolbox.com/dry-air-properties-d_973.html 2021.
[52] Macchi E, Astolfi M. Organic Rankine Cycle (ORC) Power Systems-Chapter 13-Heat transfer and heat exchangers. Woodhead Publishing; 2017.
[53] Marburg S, Nolte B, editors. Computational acoustics of noise propagation in fluids: finite and boundary element methods. Berlin: Springer; 2008.
[54] Siemens, CD-Adapco. Star-CCM+ 2020 User's Guide 2020.
[55] Defraeye T, Verboven P, Nicolai B. CFD modelling of flow and scalar exchange of spherical food products: Turbulence and boundary-layer modelling. Journal of Food Engineering 2013;114:495–504. https://doi.org/10.1016/j.jfoodeng.2012.09.003.
[56] Antebas AG, Denia FD, Pedrosa AM, Fuenmayor FJ. A finite element approach for the acoustic modeling of perforated dissipative mufflers with non-homogeneous properties. Mathematical and Computer Modelling 2013;57:1970–8. https://doi.org/10.1016/j.mcm.2012.01.021.
[57] Beltman WM. Viscothermal wave propagation including acousto-elastic interaction, part I: Theory. Journal of Sound and Vibration 1999;227:555–86. https://doi.org/10.1006/jsvi.1999.2355.
[58] Sambuc C, Lielens G, Coyette J-P. An Extension of the Low Reduced Frequency Model for Viscothermal Acoustic Propagation Within Waveguides. ASME 2012 Noise Control and Acoustics Division Conference, New York City, New York, USA: American Society of Mechanical Engineers. 2012. 285–90. doi: 10.1115/NCAD2012-0853.
[59] Hexagon FFT. Actran 2020 User's Guide Vol. 1 Installation, Operations, Theory and Utilities. 2020th ed. 2020.
[60] Farooq Anjum M, Tasadduq I, Al-Sultan K. Response surface methodology: A neural network approach. European Journal of Operational Research 1997;101:65–73. https://doi.org/10.1016/S0377-2217(96)00232-9.
[61] Box G., Hunter W., Hunter J. Statistics for experiments: Design, Innovation, and Discovery. II nd. New York: Wiley Interscience. 2005.
[62] Zolan AJ, Hasenbein JJ, Morton DP. Optimizing the design of a latin hypercube sampling estimator. 2017 Winter Simulation Conference (WSC), Las Vegas, NV: IEEE. 2017. 1832–43. doi: 10.1109/WSC.2017.8247920.
[63] Wang M, Wright J, Brownlee A, Buswell R. A Comparison Of Approaches To Stepwise Regression For Global Sensitivity Analysis Used With Evolutionary Optimization. 2013. doi: 10.26868/25222708.2013.1047.
[64] McCall J. Genetic algorithms for modelling and optimisation. Journal of Computational and Applied Mathematics 2005;184:205–22. https://doi.org/10.1016/j.cam.2004.07.034.
[65] Adeli H, Cheng N. Augmented Lagrangian Genetic Algorithm for Structural Optimization. Journal of Aerospace Engineering 1994;7:104–18. https://doi.org/10.1061/(ASCE)0893-1321(1994)7:1(104).
[66] Kyaw Oo D'Amore G, Mauro F, Rognoni G, Morgut M, Biot M. A combined CFD-FEM approach to evaluate acoustic performances of an integrated scrubber-silencer for marine applications. Genoa-La Spezia (Italy) 2022.